International Journal of Fatigue 134 (2020) 105521

Contents lists available at ScienceDirect

International Journal of Fatigue

journal homepage: www.elsevier.com/locate/ijfatigue

Effect of bead characteristics on the fatigue life of shot peened Al 7475-T7351 specimens

N. Ferreira[a], J.S. Jesus[a,*], J.A.M. Ferreira[a], C. Capela[a,b], J.M. Costa[a], A.C. Batista[c]

[a] CEMMPRE, Department of Mechanical Engineering, University of Coimbra, P-3004 516 Coimbra, Portugal
[b] ESTG, Department of Mechanical Enginnering, Instituto Politécnico de Leiria, Morro do Lena – Alto Vieiro, 2400-901 Leiria, Portugal
[c] CFisUC, Department of Physics, University of Coimbra, 3004-516 Coimbra, Portugal

ARTICLE INFO

Keywords:
Aluminium Alloys
Shot Peening
Fatigue Life Enhancement
Internal Crack Initiation

ABSTRACT

The present work aims to analyse the effect of shot peening processing parameters, material and size of beads on the fatigue behaviour of aluminium alloy AA7475-T7351. A systematic study was carried out on the roughness, surface hardening, residual stress profiles and fatigue life. Fatigue tests were carried out under both three points bending (3 PB) and tensile loadings. For 3 PB tests it was concluded that shot peening does not introduce significant improvement on fatigue life and that the use of low size glass beads is potentially beneficial, with roughness being as or more important than residual stresses. All tensile treated specimens presented an improvement of fatigue life in comparison to the untreated specimens, particularly when the crack initiated internally. Internal crack propagation generates a conical fracture surface until transition to mode I propagation.

1. Introduction

Aluminium alloys are widely used in the aerospace and aeronautical industries due to their high strength-to-weight ratio. AA7475-T7351 alloy is a new aerospace material with improved mechanical properties compared to others, such as 7050 and 7075 alloys [1–3]. Fatigue cracks initiate mainly on the surface, which explains why the preparation of the surface to resist crack initiation and earlier crack growth is an attractive method of improving fatigue performance. Shot peening is a widely used mechanical surface treatment to improve the fatigue life of metallic components. During the shot peening process the beads are bombarded into the material's surface by a nozzle. The main process parameters are: the beads size and material, Almen intensity (Almen intensity is a measure of the shot peening intensity obtained by the "Almen" test [4]) exposure time, coverage, air pressure, impact angle and nozzle characteristics [5,6]. Each impact produces local plastic deformation which expansion is constrained by the adjacent material, resulting in a field of surface compressive stresses. A positive effect of shot peening was observed in many research works [7–9], due to the introduction of compression residual stresses in the subsurface layers of the material.

As with steels, most of the improvement in the fatigue life of an aluminium alloy may be attributed to the compressive residual stresses in the surface region, which often overcompensates the worsening of the surface's morphology [10–14]. However, the increase of aluminium alloys' fatigue resistance by shot peening is more difficult to achieve. The roughness of the peened surface is generally worse, which may cancel or reduce the beneficial effect of the compressive residual stress field. Therefore, shot peening in aluminium alloys produces both balancing beneficial and detrimental effects (residual stresses and surface roughness), with the determination of optimized process parameters becoming a difficult and time-consuming task to accomplish. In order to reduce the surface roughness and enlarge compressive residual stress field, new technologies have been developed, such as laser peening [15–17] and ultrasonic peening [18,19].

In addition to the effect of surface roughness, shot peening in aluminium alloys causes the work hardening, which enhances resistance to crack initiation. On the other hand, it reduces fatigue crack propagation resistance during early crack growth due to the material's embrittlement. In addition, the material of the shot bead plays an important role on the shot peening of aluminium alloys. Using steel beads, which caused rough peened surface, Luo et al. [20], obtained only an increase of 7% in fatigue life while Sharp et al. [11], by peening with lighter materials (glass and ceramic beads), decreased surface roughness and improved the fatigue strength significantly. Recently, Benedetti et al. [21] studied the effect of shot peening treatments on the plain bending fatigue strength of aluminium alloy AA7075-T651, concluding that shot peening conducted with small beads promotes a more effective improvement of the fatigue resistance, as it causes a lower surface roughness and induces the maximum compressive residual stress in the

* Corresponding author.
E-mail address: joel.jesus@uc.pt (J.S. Jesus).

https://doi.org/10.1016/j.ijfatigue.2020.105521
Received 15 July 2019; Received in revised form 2 November 2019; Accepted 30 January 2020
Available online 31 January 2020
0142-1123/

Table 1
Chemical composition of the AA7475-T7351 aluminum alloy [% weight].

Si	Fe	Cu	Mn	Mg	Cr	Zn	Ti	Al
0.1	0.12	1.2–1.9	0.06	1.9–2.6	0.18–0.25	5.2–6.2	0.06	Remaining

region closer to the surface. These authors also obtained additional improvement of fatigue strength by eliminating surface roughness by the tribo-finishing process.

The improvement in fatigue strength due to surface peening on aluminium alloys needs to be more studied in order to enable the development of the curves' designs based on more accurate fatigue life and prediction models. The main purpose of this paper is to evaluate the effect of shot peening parameters, bead diameter and material on fatigue design curves under both 3 PB and tensile cyclic loadings in the aluminium alloy AA7475-T7351.

2. Materials and experimental procedures

Test specimens were performed from AA7475-T7351 aluminium alloy. This material was heat treated at 470 °C, then subjected to water quenching and controlled stretching from 1.5% to 3%, followed by artificial aging in two phases: first at 121 °C for 25 h and then at 163 °C in the range of 24 to 30 h. The chemical composition is indicated in Table 1, according with the specifications provided by supplier ALCOA Company. The main mechanical properties are yield stress of 414 MPa, tensile strength of 490 MPa and a maximum elongation of 9% (according to ALCOA Company).

Five batches of samples were prepared for each loading mode: an untreated reference batch was grounded with 1000 grit SiC paper and additionally polished with diamond pastes up to 1 μm; in the other four batches, the specimens' surface was submitted to shot peening treatments. Table 2 indicates the diameters and materials of the beads used in the different batches. It was assumed that the particles have spherical shape. Bead sizes are in accordance with the standard specifications and recommendations on ASM 2430 [4] for the shot peening of aluminium alloys.

Shot peening was done in OGMA - Indústria Aeronáutica de Portugal S.A., a company with great experience in surface treatment of components for the aeronautical industry, using a SURFATEC machine and with a type A Almen strip. The samples were rotated in order to promote an approximate impact angle of the beads on surfaces of 90° in all zones. The coverage of the shot peening was 100% for a Almen intensity of 0.20 A (mm), according to the ASM 2430 standard [4].

Fatigue tests were carried out using round dog bone specimens with 6 mm diameter in the center region and tested in three points bending (3 PB) under tensile loadings with the stress axis parallel to the microstructure's longitudinal direction. All tests were conducted in load control mode, at air and room temperature and at a frequency ranging from 10 to 20 Hz. Bending tests were carried out using an Instron EletroPuls E10000 machine, while for the tensile tests a 100 kN capacity Instron servo hydraulic machine was used. Tensile fatigue tests were performed at the load ratio R = 0 and the 3 PB tests at R = 0.1.

Fig. 1(a)–(c) show the geometry of the tensile tests, a schematic view of the apparatus for 3 PB tests and the geometry of the 3 PB test specimens, respectively. For the tensile tests, the load amplitude and mean load required as input data were calculated as $P_a = P_m = \sigma_a A$, while for 3 PB tests the amplitude load was calculated taking into account the values of the nominal bending stresses, according to Eq. (1):

$$P_a = \frac{\pi D^3 \sigma_a}{16L} \quad (1)$$

where σ_a is the stress amplitude, P_a is the bending or axial load amplitude, L is the specimen span, D is the diameter of the specimen and A the cross section area.

Table 2
Parameters for the different shot peening batches.

Code	Bead material	Mean bead size (μm)	Standard deviation size (μm)
Polished	–	–	–
GB8	Glass	166	28
GB35	Glass	377	32
SB110	Iron	348	21
SB170	Iron	670	75

One specimen of each batch was cut through a plane containing longitudinal axle and afterwards the surface was gradually polished with smaller granulometry silicon carbide papers, while at the end diamond particles with a 1 μm diameter were used until the surface became mirror-like. Afterwards, said surfaces were etched with Keller reagent (2.5% HNO_3; 1.5% HCl; 1% HF; 95% H_2O) and observed with an optical microscope Leica DM 4000 M LED.

The roughness evaluation was carried out according to the DIN EN ISO 4288 [22] standard using the rugosimeter Mitutoyo, Surftest SJ-500. Vickers nanohardness measurements were performed in cross section specimens using a Berkovich three-sided diamond pyramid indenter with a half angle of 65.35°. The maximum load applied was 30 mN. The equipment has a load and displacement resolution of 0.5 mN and 80 nm, respectively. The wait time was 5 s while the loading and unloading time was 10 s. Measurements started at a distance from surface of 5 μm with increments of 20 μm up to 185 μm depth. An additional test was also performed at the center of the specimen to estimate the base material's nanohardness value.

The residual stress analysis was performed by X-ray diffraction using a Proto iXRD equipment in the longitudinal direction of the samples. Lattice deformations of the {2 2 2} diffraction planes ($2\theta \approx 157°$) were measured using Cr-K_α X-ray radiation, with 21 β angles in the range ± 30° (42 ψ angles in the range ± 42°), an acquisition time of 60 s by peak and ± 2° oscillations in ψ. The stress was evaluated with an elliptical regression of $\sin^2\psi$ data and the X-Ray elastic constants values of 18.56×10^{-6} MPa^{-1} for $(1/2)\cdot S_2$ and -4.79×10^{-6} MPa^{-1} for S_1. For the analysed material, and considering the radiation used, the average penetration depth of the X-Rays was about 11 μm. The analysis of the in-depth evolution of the residual stresses was performed step-by-step, by removing successive thin layers of material by electrolytic polishing. For some of the deeper layers both ψ and φ oscillations were used, to get better diffraction peak profiles.

Finally, the fatigue fractured surfaces of the broken specimens were analysed with a scanning electron microscope (SEM), Philips® XL30 TMP.

3. Results and discussion

3.1. Metallographic analysis

The region near the surface was observed by optical microscopy in order to study the shot peening's effect on the microstructure. Fig. 2(a)–(e) shows exemplary photos. Fig. 2(a) shows the microstructure of the aluminum alloy, presenting the grains elongated in the rolling direction, typical of extruded rods. Fig. 2(b) and (c) highlight the surface area where the shot peening occurred in the cases of steel beads, SB170 and SB110, respectively. It was noticed that SB170 and SB110 steel beads, which have a much higher mass than glass beads, promote a larger damaged area (presenting a surface damaged layer with about 100 μm depth). A visual analysis of Fig. 2(c) and (d) seems to indicate that SB110 and GB35 beads have similar roughness, lower than SB170 series, and a few surface defects, with a significantly lower depth than the plastically deformed layer created by the shot peening treatment, which may promote the onset of fatigue cracking. Fig. 2(e) shows that GB8 beads reduced significantly the plastic deformed layer and the roughness in comparison with the other shot peening series. On

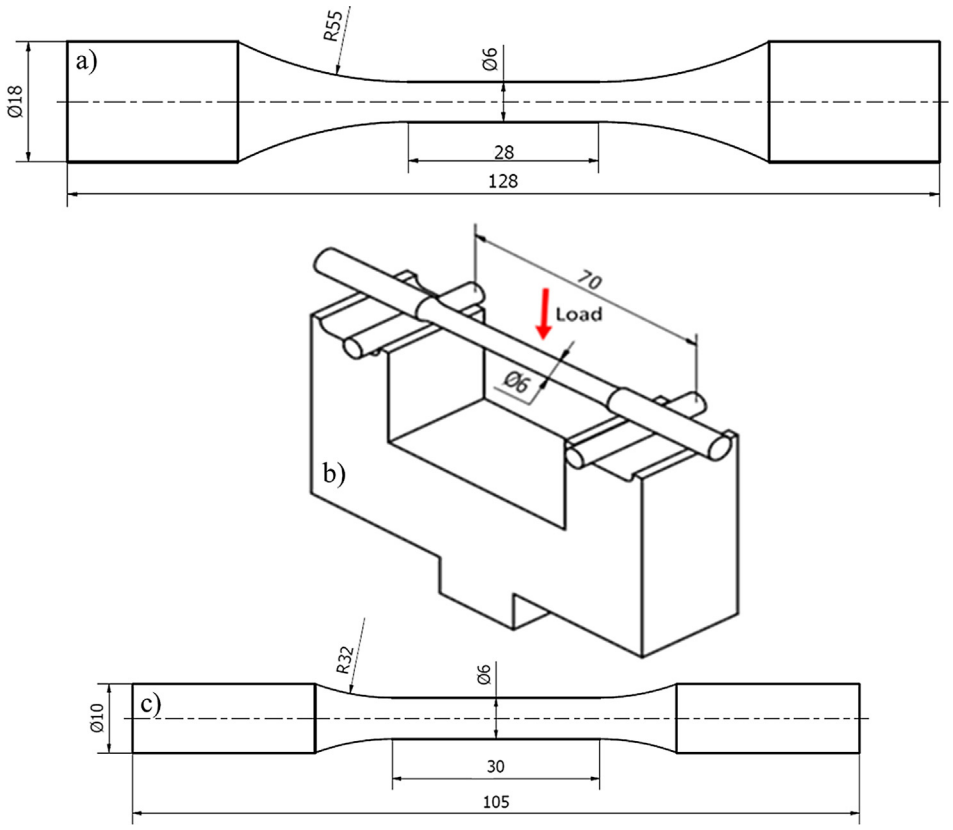

Fig. 1. (a) Geometry of the tensile test specimens; (b) 3 PB testing apparatus; (c) Geometry of 3 PB tests specimens. (Dimensions in mm).

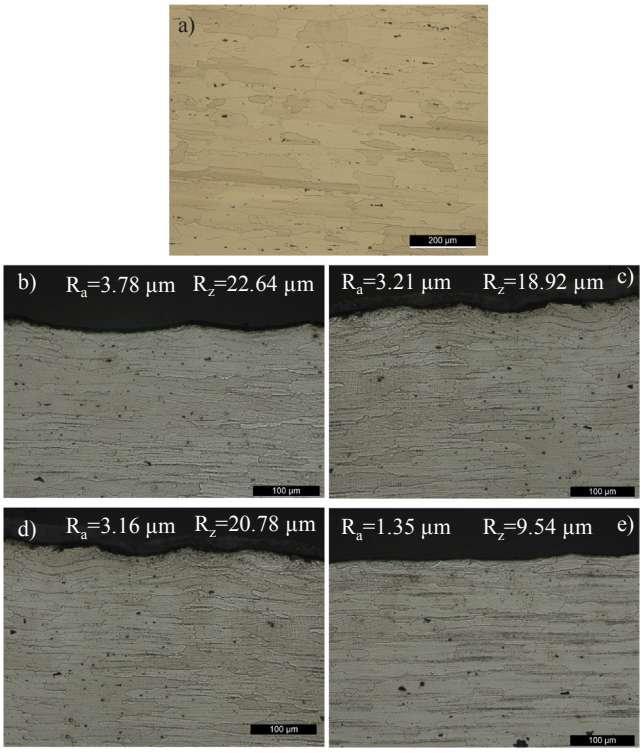

Fig. 2. Microstructures: (a) Aluminum alloy; (b) Peened with SB170; (c) Peened with SB110, (d) Peened with GB35; (e) Peened with GB8.

Table 3
Roughness parameters for the treated and untreated series.

Series	Rougness	Average	Standard Deviation	k_t	k_f
GB8	Ra [µm]	1.35	0.096		
	Ry [µm]	11.78	0.994		
	Rz [µm]	9.54	0.524		
	D_p [µm]	98.10	2.686	1.204	1.028
GB35	Ra [µm]	3.16	0.155		
	Ry [µm]	26.21	1.976		
	Rz [µm]	20.78	1.816		
	D_p [µm]	221.95	9.218	1.197	1.053
SB110	Ra [µm]	3.21	0.350		
	Ry [µm]	25.69	3.642		
	Rz [µm]	18.92	2.390		
	D_p [µm]	162.67	5.104	1.244	1.062
SB170	Ra [µm]	3.78	0.277		
	Ry [µm]	30.78	3.512		
	Rz [µm]	22.64	2.342		
	D_p [µm]	367.62	7.761	1.129	1.051
Non treated	Ra [µm]	0.06	0.011		
	Ry [µm]	0.49	0.131		
	Rz [µm]	0.41	0.080		

the other hand, a visual analysis of Fig. 2(d) did not reveal the presence of surface defects in the GB8 specimens.

3.2. Roughness evaluation

The roughness parameters evaluated for each superficial treatment are summarized in Table 3: roughness average R_a, maximum peak-to-valley height R_y, the average maximum peak to valley of five consecutive sampling lengths within the measuring length R_z, the average spacing of adjacent peaks in the surface profile D_p, the elastic stress

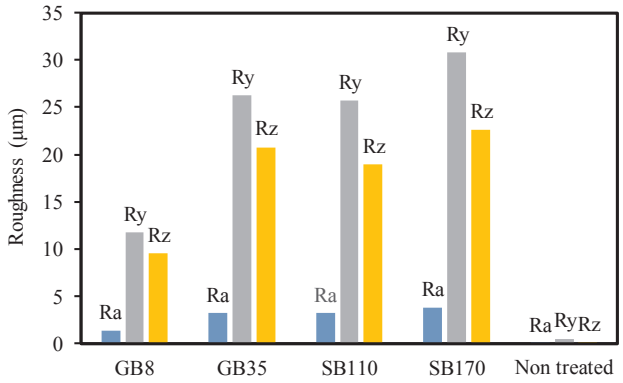

Fig. 3. Average roughness parameters for the different batches.

concentration factor k_t and the notch factor k_f. The elastic stress concentration factor k_t, introduced by multiple micro-notches after shot peening, according to Li et al. [23] is given by Eq. (2):

$$k_t = 1 + 2.1\left(\frac{R_z}{D_p}\right) \tag{2}$$

and the notch factor k_f can be calculated by the Peterson formulation, Eq. (3):

$$k_f = 1 + \frac{k_t - 1}{1 + \frac{a}{r}} \tag{3}$$

where a and r are a material characteristic length of the crack initiation processing zone and the mean radius of beads indicated in Table 2, respectively. For aluminium alloys a is estimated as 0.51 mm.

Fig. 3 shows the average of roughness parameters for the different batches used in 3 PB and tensile tests. The roughness values indicated in Fig. 3, along with the images shown in Fig. 2, indicate that even the higher roughness caused by SB170 beads presents a smoother surface profile with fewer localized notches when compared to GB35 and SB110 beads.

Table 3 and Fig. 3 show that the shot peening treatments increase the surface roughness relatively to the untreated specimens and that the steel SB110 and SB170 beads and glass GB35 beads produce similar and significantly higher levels of roughness than GB8 beads. In all cases it can be said that the layer treated by shot peening is very shallow, affecting only a few surface grains with a depth which is generally less than 100 µm.

3.3. Hardness analysis

Shot peening promotes surface densification, the increase of hardness and the accumulation of compressive residual stresses. Fig. 4 presents the averages of hardness of all indentions performed around the surface for the different samples batches. All series show a similar trend, with a slight increase (lesser than 10%) in surface hardness and a progressive attenuation of the effect of the impact of the beads until they converge to the hardness of the base material of about 246 HV to about 200 µm depth. The GB8 series presents the lower values of hardness for depths until 60 µm. These results partially coincide with those obtained by Ramos et al. [19] for the same material, which also found only a slight increase of hardness in the shot peened surface in comparison with the base material, due to the cold work and the consequent plastic deformation induced by the beads' impact.

3.4. Residual stresses evaluation

The surface and in-depth measurements of residual stresses in the longitudinal direction are shown in Fig. 5. Fitted residual stress profiles of the shot peened series using the Robertson formula [24] are also

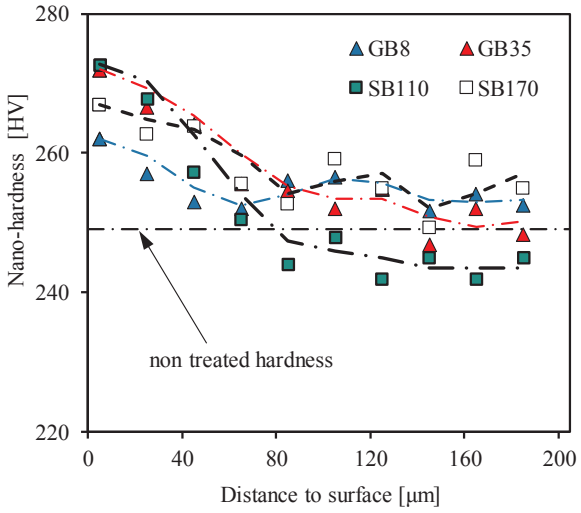

Fig. 4. In depth hardness distribution for the different beads.

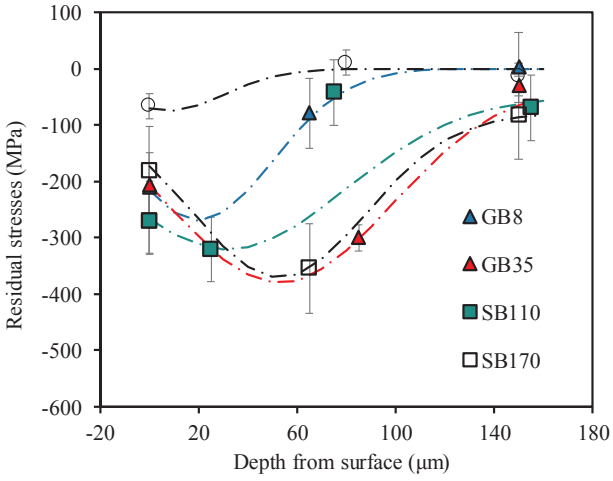

Fig. 5. In depth residual stresses for the different beads.

superimposed, as seen in Eq. (4):

$$\sigma_{res} = A \cdot exp\left(\frac{-2(x - x_2)^2}{W^2}\right) + B \tag{4}$$

where σ_{res} is the residual stress, x, the depth below the surface, $A + B$, the maximum residual stress, W, a measure of the width of the curve and x_d, is the depth to the maximum residual stress.

All surface treatments induce compressive residual stresses on the surface layer, which is the first measurable layer by X-Ray diffraction at a depth of 11 µm. The values obtained for the surface residual stresses are indicated in Table 4.

Shot peening treatments increased the surface residual compressive stresses to values in the range 180–270 MPa. However, it was not possible to establish a direct connection between the residual stresses values and the diameter of the beads or the impact energy.

Table 4
Residual stress values on the surface.

Treatment	Residual Stress [MPa]
Polished	−66 ± 14
GB8	−210 ± 9
GB35	−206 ± 6
SB110	−271 ± 6
SB170	−181 ± 3

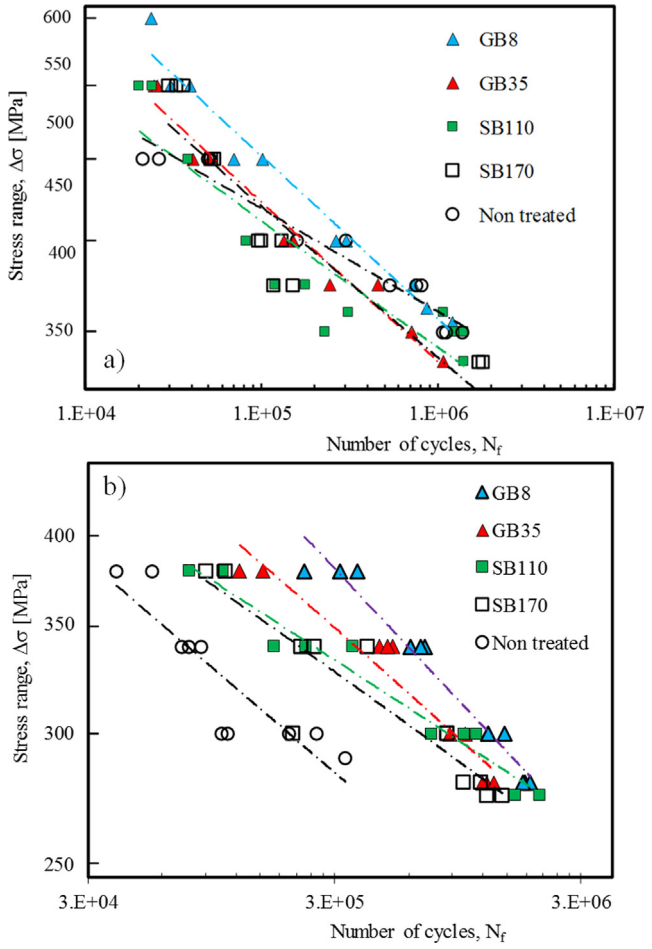

Fig. 6. S-N curves for the batches with different shot peening beads and the reference polished samples: (a) 3 PB tests; (b) Tensile tests.

A more detailed observation of the results plotted in Fig. 5 indicated that they agree with those obtained by Gao [17], showing that the maximum compressive residual stresses did not occur at the surface but at inner layers with about 25–60 μm depth, depending of the beads' type. Regardless of the bead type used in shot peening, the residual stresses caused by the impacts tends to zero for about 150 μm depth.

3.5. Fatigue tests results

The results of the fatigue tests are shown in Fig. 6(a)–(b) in terms of the stress amplitude against the number of cycles to failure, comparing the S-N curves for shot peened series with polished specimens for 3 PB tests and tensile tests, respectively. As is well known, fatigue crack initiation is a localized process, causing a significant dispersion of results by the combined effect of the residual stresses, hardness and roughness.

The S-N curves were fitted using Basquin's law, Eq. (5):

$$\sigma_a = \sigma_f' \times (N_f)^b \quad (5)$$

where: σ_f' is the cyclic resistance coefficient, b is the cyclic resistance exponent and N_f the number of cycles to failure. The values of σ_f' and b are summarized in Table 5 for all the series tested. Table 5 also presents the fatigue resistance improvement of the different treatments, for a fatigue life of 5×10^5 cycles, in comparison with simply polished specimens.

For a fatigue life of 5×10^5 cycles, the 3 PB fatigue resistance of GB8 series is similar of the untreated series, while the other treated series present slightly lower resistances to fatigue. As expected, in all specimens tested in 3 PB loading the crack initiation occurs from the surface, due to the high stress gradient created by the bending loading. For lower lives the GB8 series show better fatigue performance than untreated series. The only parameter where GB8 series present better results than the other series is the roughness (see Fig. 3 and Table 3). In what concers the residual stresses and hardness profile, all series present similar values. The S-N curves obtained for the other treated series present lower resistance than the untreated series for fatigue lives above 10^5 cycles. Despite the increase of surface hardness and the introduction of compressive residual stresses in a surface layer with 150 μm depth, the shot peening treatment did not produce a beneficial effect with GB35, SB110 and SB170 beads. It seems that with 3 PB tests the roughness has a detrimental effect, equivalent to the potential beneficial effect of the compressive residual stresses resulting from the shot peening. Therefore, it can be concluded that the shot peening treatment does not introduce significant improvement on fatigue life and that the use of small glass beads is potentially beneficial for specimens tested in 3 PB.

Table 5
Analysis of the S-N Curves for all treatments.

Treatment	σ_f' [MPa]	b	Loading mode	Improvement [%]*
Non treated	457	−0.058	3 PB	–
GB8	718	−0.091	3 PB	2
GB35	668	−0.09	3 PB	−4
SB110	528	−0.072	3 PB	−4
SB170	632	−0.086	3 PB	−4
Non treated	1169	−0170	Tensile	–
GB8	1987	−0.184	Tensile	42
GB35	2459	−0.204	Tensile	35
SB110	896	−0.130	Tensile	30
SB170	1968	−0.189	Tensile	31

* (in relation to polish specimens for 5×10^5 cycles).

Table 6 summarizes the fatigue results obtained in the tensile tests. The number of cycles N_{est} was calculated from Eq. (5) for each value of the stress range. For the majority of the specimens, crack initiation occurs internally at the depth *f* indicated in this table. For the GB8 series internal crack initiation occurs 92% of times, for the GB35 series 80%, and for SB110 and SB170 series 55%.

In the case of fatigue tensile tests, the S-N curves, presented in Table 5 and plotted in Fig. 7, were fitted using only the fatigue results obtained with the specimens with internal crack initiation.

A very good coefficient of correlation of R above 0.98 was obtained, except for the SB110 series. The GB8 series present the higher fatigue lives (about 7.3x superior to the untreated material for a stress range of 300 MPa), while the other treated series present similar fatigue resistances with fatigue lives about 5x also superior to the untreated material. For a fatigue life of 5×10^5 cycles, the GB8 series has an increase of fatigue resistance of 42% relatively to the untreated series. The others treated series present a lower increase of fatigue resistance between 30 and 35%. Therefore, in the case of tensile fatigue tests, all shot peening treatments lead to an important increase of fatigue life in the range of stresses used in the tests, 275–380 MPa, when the crack initiation occurs internally. The GB8 series present the lowest value of roughness and Table 3 shows that this series also presents the lower value of k_f, although the same is not very different from the values obtained for the others treated series. This is in agreement with the higher fatigue performance presented by the GB8 series. In addition, the very low values obtained for the notch factor k_f, the presence of compressive residual stresses on the surface layer and the uniform stress distribution in tensile loadings justify the higher percentage of specimens that fail from internally initiated cracks under tensile loading. The stress intensity factor ΔK_I, considering an internal defect as a crack, may be calculated by an approximate equation from Murakami [25], Eq. (6):

$$\Delta K_I = \beta \Delta\sigma \sqrt{\pi \sqrt{A}} \quad (6)$$

Table 6
S-N curves parameters.

Ref.	Δσ [MPa]	f [mm]	N_f [cycles]	N_{est} [cycles]	N_f/N_{est}	Ref.	Δσ [MPa]	f [mm]	N_f [cycles]	N_{est} [cycles]	N_f/N_{est}
GB8_1	300	1.18	1,261,038	1,275,635	0.989	SB110_1*	300	0.00	293,943	939,865	0.313
GB8_2	340	0.93	695,965	645,628	1.078	SB110_2*	340	0.00	171,484	358,716	0.478
GB8_3	380	0.23	371,161	352,510	1.053	SB110_3*	380	0.00	77,102	152,411	0.506
GB8_4	280	2.25	1,783,084	1,856,724	0.960	SB110_4	275	0.45	2,050,486	1,835,994	1.117
GB8_5	380	0.22	315,074	352,510	0.894	SB110_5	300	1.30	741,971	939,865	0.789
GB8_6	340	0.79	609,907	645,628	0.945	SB110_6	275	0.90	1,627,259	1,835,994	0.886
GB8_7	300	1.33	1,466,090	1,275,635	1.149	SB110_7*	340	0.00	230,404	358,716	0.642
GB8_8*	380	0.00	227,562	352,510	0.646	SB110_8*	380	0.00	106,510	152,411	0.699
GB8_9	340	0.90	673,857	645,628	1.044	SB110_9	300	1.68	1,003,861	939,865	1.068
GB8_10	300	1.29	1,256,335	1,275,635	0.985	SB110_10	340	0.25	356,328	358,716	0.993
GB8_11	280	2.31	1,862,700	1,856,724	1.003	SB110_11	300	1.12	1,126,466	939,865	1.199
GB8_12	280	2.12	1,736,114	1,856,724	0.935	SB170_1	300	0.99	858,755	815,102	1.054
GB35_2	340	1.06	455,600	492,120	0.926	SB170_2	340	0.93	407,785	420,550	0.970
GB35_3	340	1.13	516,811	492,120	1.050	SB170_3	280	2.22	999,830	1,173,899	0.852
GB35_4*	380	0.00	123,869	285,166	0.434	SB170_4*	380	0.00	90,803	233,575	0.389
GB35_5*	380	0.00	154,602	285,166	0.542	SB170_5*	340	0.00	113,763	420,550	0.271
GB35_6	300	0.91	878,902	909,366	0.967	SB170_6*	340	0.00	97,062	420,550	0.231
GB35_7	300	1.00	1,019,929	909,366	1.122	SB170_7	280	2.90	1,178,237	1,173,899	1.004
GB35_8	280	1.73	1,248,000	1,275,652	0.978	SB170_8*	380	0.00	108,165	233,575	0.463
GB35_9	280	1.59	1,191,270	1,275,652	0.934	SB170_9	300	1.04	857,158	815,102	1.052
GB35_10	280	1.94	1,328,353	1,275,652	1.041	SB170_10	275	0.58	1,437,863	1,291,232	1.114
GB35_11	340	1.10	492,775	492,120	1.001	SB170_11	275	0.39	1,253,275	1,291,232	0.971
						SB170_12*	300	0.00	204,174	815,102	0.250

* Surface crack initiation.

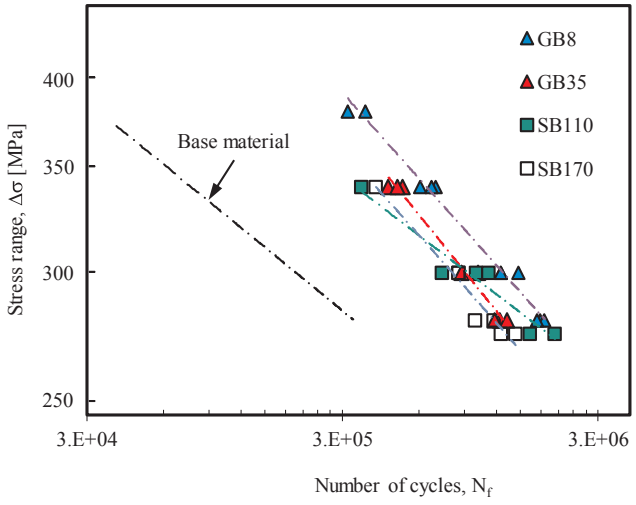

Fig. 7. S-N curves for the batches with different shot peening beads. Tensile tested specimens with internal crack initiation.

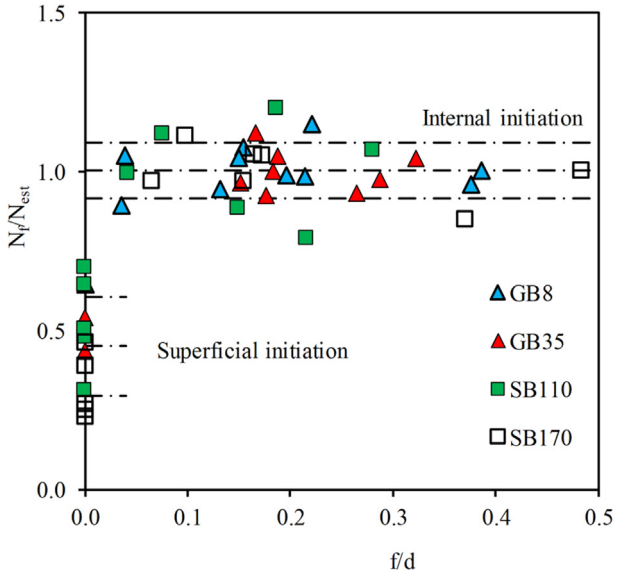

Fig. 8. N_f/N_{est} against normalized crack initiation depth f/d for the batches with different shot peening beads. Tensile tests.

where A is the area of the defect projected in the plane normal to the tensile stress, β = 0.5 for an internal defect and β = 0.65 for a surface defect. Therefore, for a given applied stress range, ΔK_I is about 1.3 higher for a surface defect than for an internal defect with the same size. The difference between β values for internal and surface defects and the usually accepted idea that vacuum makes crack growth slower and the threshold higher agree with the results obtained in tensile fatigue tests in Table 4, which shows an increase of fatigue resistance between 1.3 and 1.42 for treated specimens that failed from internal crack initiation relatively to untreated specimens which failed from surface crack initiation.

The ratio between the experimental number of cycles N_f and N_{est} (Table 6) is used to quantify the deviation between the total fatigue lives of specimens with surface crack initiation and the total fatigue lives of specimens with internal crack initiation, for the same stress range. Fig. 8 shows the ratio N_f/N_{est} against the ratio f/d, where d is the specimen diameter. For internal crack initiation, N_f/N_{est} has an average value near unity and a standard deviation of 0.088, while for surface initiation these parameters change to 0.45 and 0.166, respectively. It can be concluded that fatigue life increases in average 2.2x when crack initiation occurs internally in comparison to surface crack initiation. However, even in the case of specimens with surface crack initiation there is an increase of fatigue resistance relatively to the untreated series, as can be observed in Fig. 6(b).

The improvement difference introduced by the shot peening process on bending and tensile test results is caused by the different stress distributions created by bending and tension loadings, leading to different fatigue resistances.

The fatigue strength obtained in the 3 PB tests was higher than that obtained in tensile tests, particularly for long lives where the initiation phase is predominant. The strong stress gradient and the restricted volume subjected to higher stresses in specimens tested under 3 PB loading are the main causes for its higher fatigue resistance and also explain that crack initiation always occurred on the specimen surface.

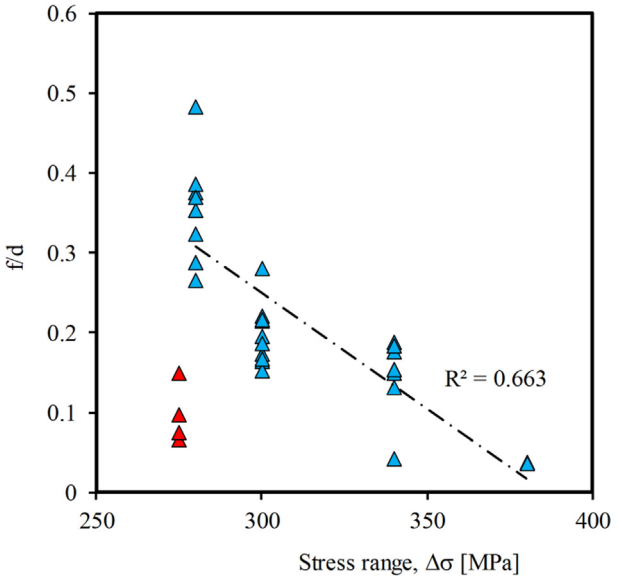

Fig. 9. Normalized crack initiation depth f/d against stress range for the batches with different shot peening beads. Tensile tests.

As indicated in Table 5, the slope of S-N curves for 3 PB tests is very low (−0.058 to −0.09), indicating that the crack initiation phase is predominant in the total fatigue life. Moreover, the maximum stress applied in 3 PB tests ranged from 385 to 600 MPa, which is typically greater than the microscopic yield strength (the microscopic yield strength of the material surface is lower than the global yield strength of 414 MPa) and reduces or eliminates the residual stress field with a maximum depth of 140 μm. Consequently, in 3 PB tests the favorable effect of the compressive residual stresses on fatigue strength was canceled or reduced, leading to surface roughness and the slight increase of hardness became the main parameter that may influence the fatigue strength. For longer lives, the increase of surface roughness effect leads to a reduction in fatigue strength of some treated series compared to the untreated series.

In the case of tensile tests, a uniform stress distribution over the entire specimen volume reduced both crack initiation and propagation phases compared to 3 PB tests, leading to a reduction of the fatigue strength. Moreover, the slope of S-N curves obtained in tensile tests, being higher than in 3 PB tests (−0.13 to −0.204), indicates that the crack initiation period is lower.

The uniform distribution of stresses over the entire specimen volume makes it possible to initiate the crack superficially or internally, depending on the superficial parameters: residual stresses and roughness. As the fatigue strength was lower in tensile tests, the applied stress ranges were also smaller; the maximum stress ranged from 275 to 380 MPa, always lower than the yield stress of 414 MPa. Therefore, in the case of fatigue tensile tests the compressive residual stresses and eventually the increase of hardness near surface have a higher beneficial effect in the fatigue lives of treated series than the detrimental effect of the roughness. In spite of this, the fatigue strength in tensile tests was significantly lower than in 3 PB tests, for both treated and untreated specimens.

Dong et al [26] also achieved an extension in fatigue lifetime due to the failure mode transition from surface crack initiation to internal crack initiation on the FSW joint of the 7075-T651 aluminum alloy, by performing uniaxial fatigue tests in specimens with near-polished, gradient nanostructured surface and high compressive residual stresses provided by a surface mechanical rolling treatment. He et al [27] studied the effect of ultrasonic peening treatment on the high and very high cycle fatigue resistance of an AA7075 friction stir welded joint.

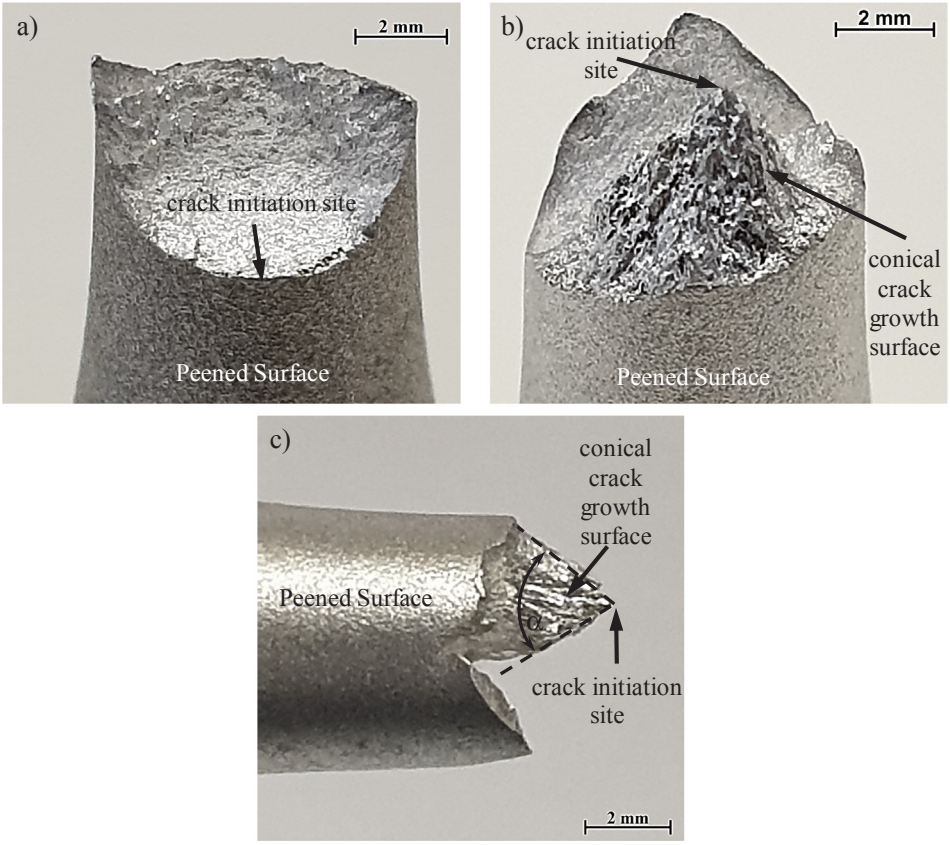

Fig. 10. Macro images of fracture surfaces in treated series: (a) crack initiation in S110_11 specimen (b) internal crack initiation in GB8_11 specimen and (c) a lateral image of the conical crack growth surface of GB8_11 specimen.

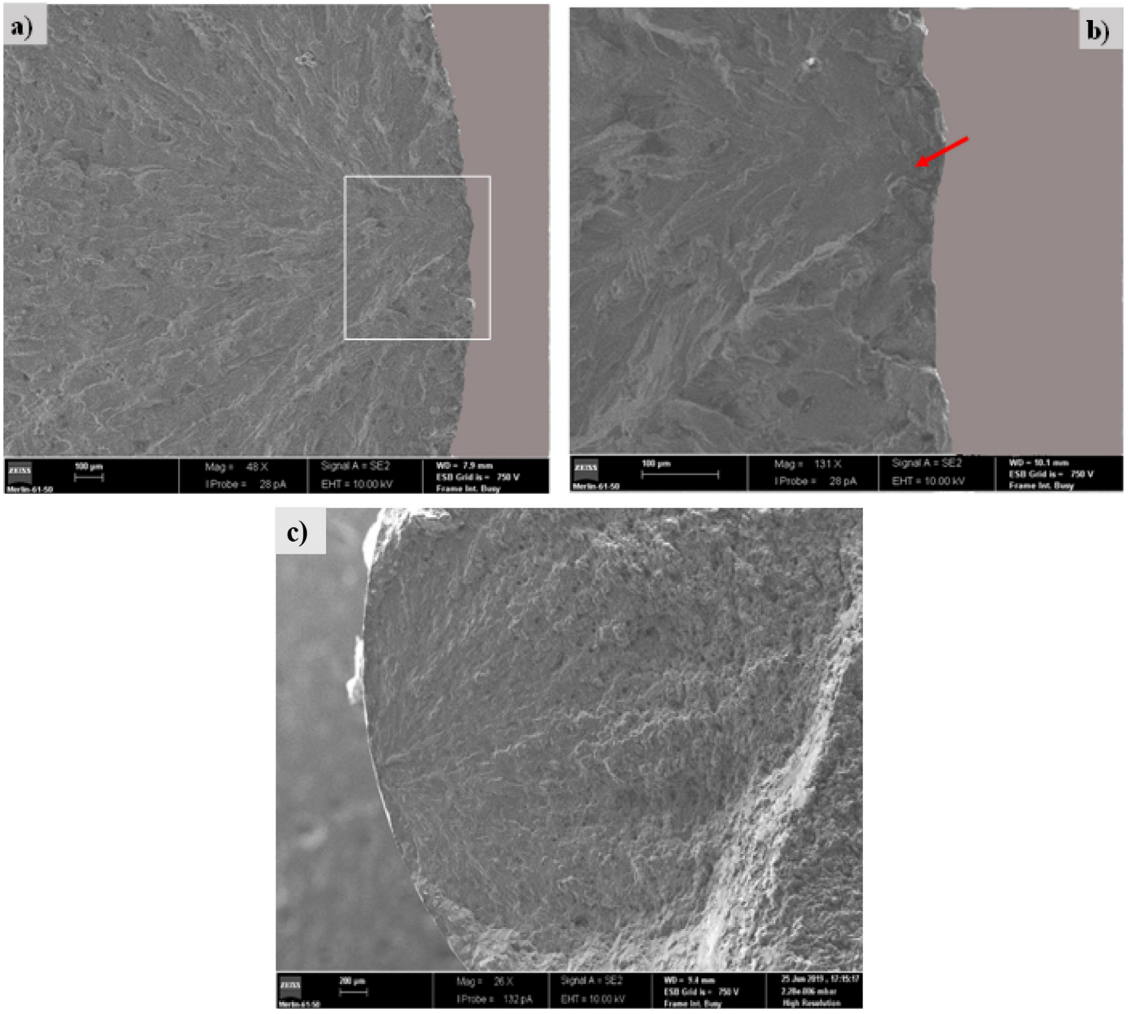

Fig. 11. SEM images of a surface crack initiation in SB110_2 tensile specimen. $\Delta\sigma = 340$ MPa: (a) Macrograph of fracture surface, (b) Detail of the crack initiation zone and (c) SEM images of a surface crack initiation in Al_3 non treated tensile specimen. $\Delta\sigma = 340$ MPa.

They also observed a fatigue strength improvement through application of ultrasonic peening treatment and that fatigue cracks can initiate from the interior of the specimen due to the compressive residual stress profile in the surface layers.

Fig. 9 presents the crack initiation dimensionless depth f/d, where d is also the specimen diameter, against the stress range for all treated series. With exception of the results for the stress range of 275 MPa, a clear trend of an increase of the crack initiation depth with the decrease of the applied stress range may be observed. The cause for the different behaviour of specimens tested with the lowest stress range (275 MPa) was not understood.

3.6. Fracture surface analysis

Fig. 10 shows two macro images of both surface crack initiation (Fig. 10(a)) and internal crack initiation (Fig. 10(b)) in treated series. Internal crack initiation occurs due to the increase of surface crack initiation resistance promoted by the compressive residual stresses, for fatigue lives above 3.5×10^5 cycles.

For fatigue lives below 3.5×10^5 cycles crack initiation always occurs at surface. Internal crack initiation occurs at the vertices of the conical surface located internally, marked by an arrow in Fig. 10(b). Fig. 10(c) shows a lateral image of this conical shape evolution of the crack with internal initiation for the tensile tested specimens. The angle of the cones ranged between 61° and 76°. After the internal crack initiation period, the crack propagates forming the conical shape surface, which size depends on the location of the start point of the crack: the farther the starting point of the crack was from the specimen surface, the larger the conical surface. Therefore, the height of the cones tend to increase with the initial crack distance to surface. The transition from the conical surface to a flat surface, corresponding to mode I crack propagation, occurs when the point of the base of the cone closest to the specimen surface reaches it. The crack shape evolution shown in Fig. 10(c) is completely different from the usually reported in literature for internal cracks that propagate in mode I with the typical eye of fish aspect. A description of this phenomenon was not found in literature, neither in aluminium alloys nor in other metallic materials.

The surface fracture analysis by SEM was performed only for the fatigue tensile specimens, where both surface and internal crack initiation occurred. In all 3 PB treated specimens the crack always initiated on the surface and propagated through the cross section. Figs. 11 and 12 show SEM images of fatigue fractured specimens with surface crack initiation and internal crack initiation, respectively. Fig. 11(a) shows a macrograph of the fracture surface for the SB110_2 tensile specimen with a total fatigue life of 171,484 cycles for a stress range of 340 MPa. The white square identifies the crack initiation site from where radial marks following the direction of crack propagation are clearly visible. Fig. 11(b) shows a detail of the crack initiation site. The red arrow indicates the crack initiation origin identified by the convergence of the radial marks. Fig. 11(c) shows a macrograph of the fracture surface for the tensile specimen Al-3 of the untreated series. Crack initiation in untreated series occurs always at the specimen

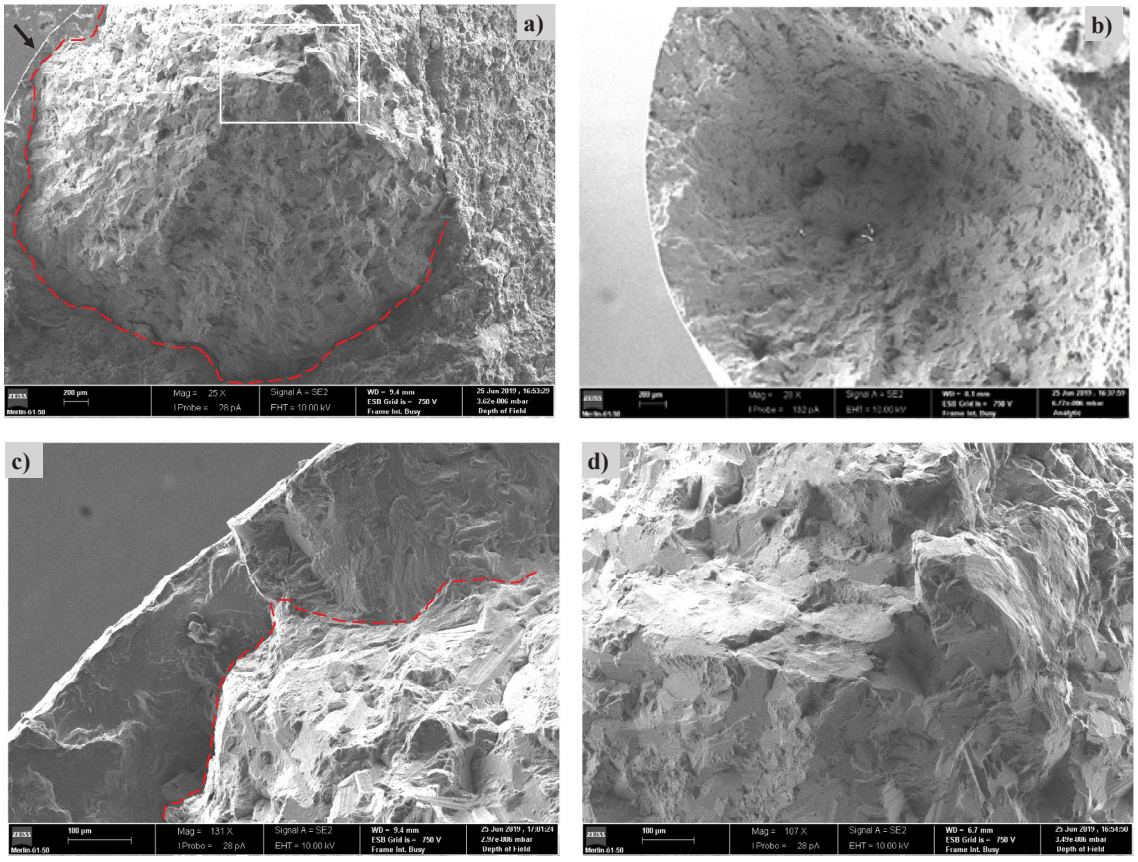

Fig. 12. SEM images of an internal crack initiation in treated series showing internal crack initiation on a conical shape surface: (a) Macrography of the fracture surface of SB110_9 tensile specimen. $\Delta\sigma = 300$ MPa; (b) Macrography of the fracture surface of GB8_11 tensile specimen. $\Delta\sigma = 280$ MPa; (c) Detail of the internal crack initiation zone of (b) and (d) Detail of transition zone between conical crack growth shape and propagation in mode I of image (b).

surface. The fracture surface aspect is similar to the one obtained with the treated series S110, but the fatigue life was lower (86,833 cycles). Although the field of compressive residual stresses introduced by shot peening in the S110 series is insufficient to prevent surface cracking initiation, it has a favorable effect on fatigue life of this treated series, increasing the initiation period.

Fig. 12(a)–(b) show macrographs of the fracture surface of two different treated series (S110 and GB8), showing internal crack initiation on a conical shape surface. The overall appearance of both fracture surfaces is similar as well the micromechanisms, which will be analyzed further below. In Fig. 12(a) the black arrow indicates the contour of the specimen cross section. The white square identifies the crack initiation site from where the crack propagates, generating a conical fracture surface which boundary is marked by the dashed red line. This line also defines the transition between the crack propagation along the conical surface and the propagation in mode I in a plane approximately normal regarding the tensile stress. Fig. 12(c) shows a detail of the crack initiation site corresponding to the cone vertices. It was not possible to identify precisely the crack initiation site. It seems that early crack growth occurs on a small plateau before changing to the conical surface shape. Fig. 12(d) shows a detail, near the surface of the specimen, of the transition zone between conical crack growth shape and propagation in mode I. As previously mentioned, this transition occurs when the nearest zone of the base of the cone approximates to the surface of the specimen allowing the contact with external environment. The multiplane aspect of crack propagation in mode I is a consequence of the irregularity of the cone base at the moment of the transition.

Fig. 13 shows SEM images of the fractured surface of the GB8-11 specimen with internal crack initiation, showing the crack propagation micromechanisms. Fig. 13(a) shows that crack propagation on the conical surface occurs by micro cleavage, while Fig. 13(b) shows a macrography and a detail of the subsequent mode I fracture zone of crack propagation, showing ductile striations and secondary cracks.

4. Conclusions

A systematic study was carried out regarding the roughness, surface hardening and residual stress effects on fatigue life on round specimens of AA7475-T7351 aluminum alloy tested under 3 PB and tensile-tensile. The main conclusions drawn were the following:

- No significant hardening near surface caused by shot peening was observed;
- For 3 PB specimens, the surface roughness plays a role as or more important than the residual stresses resulting from shot peening resulting in a surface crack initiation, while for tensile specimens the combination of these factors and the uniform stress distribution in tensile loading leads to a predominant internal crack initiation;
- Shot peening does not introduce significant improvement on fatigue life in 3 PB specimens, but the use of small glass beads is potentially beneficial. All tensile treated specimens present an improvement of fatigue life in comparison with the untreated specimens, particularly when the crack initiates internally;
- The internal cracks propagate generating a conical fracture surface until transition to mode I propagation.

Declaration of Competing Interest

The authors declare that they have no known competing financial interests or personal relationships that could have appeared to

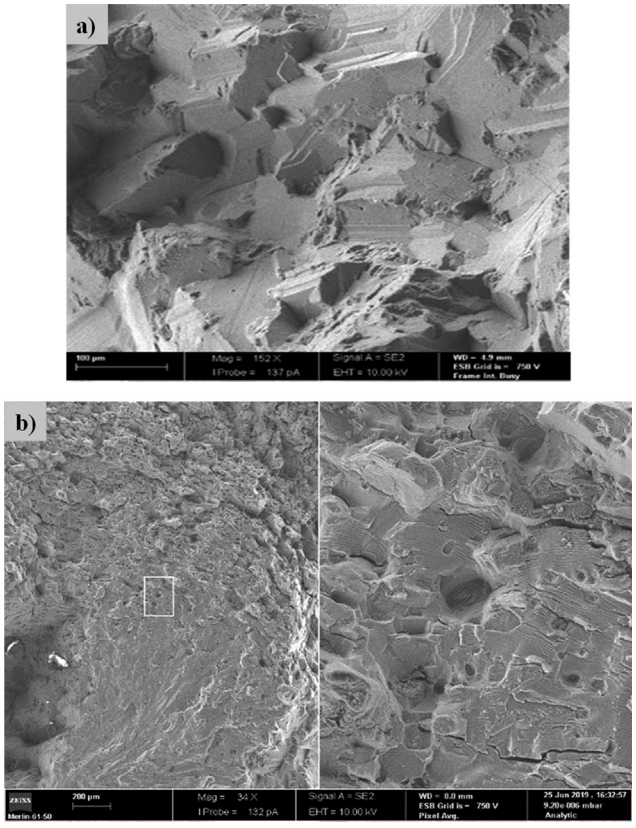

Fig. 13. SEM images showing the fatigue crack propagation micromechanisms of specimen GB8-11 with internal crack initiation: (a) Microcraph of the conical surface fracture and (b) Macrocraph and a detail of fracture on mode I crack propagation.

influence the work reported in this paper.

Acknowledgements

The authors would like to acknowledge OGMA-Indústria Aeronáutica de Portugal, in Alverca, for the collaboration in the supplying of samples used in this project, as well as FEDER for the sponsoring by way of funds through the program COMPETE – Programa Operacional Factores de Competitividade – and by national funds through FCT – Fundação para a Ciência e a Tecnologia under the project identified with the number UID/EMS/00285/2013.

References

[1] Heinz A, Haszler A, Keidel C, Moldenhauer S, Benedictus R, Miller W. Recent development in aluminium alloys for aerospace applications. Mater Sci Eng, A 2000;280(1):102–7.
[2] Kim CY, Choi JM, Song JH. Fatigue crack growth and closure behavior under random loadings in 7475–T7351 aluminum alloy. Int J Fatigue 2013;47:196–204.
[3] Alrubaie K, Barroso E, Godefroid L. Fatigue crack growth analysis of pre-strained 7475–T7351 aluminum alloy. Int J Fatigue 2006;28(8):934–42.
[4] SAE AMS 2430, Shot Peening, Automatic AMS2430, SAE International, 1948; 4.
[5] Miková K, Bagherifard S, Boků̊vka O, Guagliano M, Trško L. Fatigue behavior of X70 microalloyed steel after severe shot peening. Int J Fatigue 2013;55:33–42.
[6] Kumar H, Singh S, Kumar P. Modified Shot Peening Processes – A Review. Int J Eng Sci Emerg Technol 2013;5(1):12–9.
[7] Lundberg M, Peng RL, Ahmad M, Vuoristo T, Bäckström D, Johansson S. Influence of Shot Peening Parameters on Residual Stresses in Flake and Vermicular Cast Irons. Mater Sci Forum 2013;768–769:534–41.
[8] Bagherifard S, Guagliano M. Fatigue behavior of a low alloy steel with nanostructured surface obtained by severe shot peening. Eng Fract Mech 2012;81:56–68.
[9] Zhang P, Lindemann J, Leyens L. Shot peening on the high-strength magnesium alloy AZ80 – effect of peening media. J Mater Process Technol 2010;210:445–50.
[10] Mutoh Y, Fair GH, Noble B, Waterhouse RB. The effect of residual stresses induced by shot peening on fatigue crack propagation in two high strength aluminium alloys. Fatigue Fract Eng Mater Struct 1987;10(4):261–72.
[11] Sharp PK, Clayton JQ, Clark G. The fatigue resistance of peened 7050–T7451 aluminium alloy-repair and retreatment of a component surface. Fatigue Fract Eng Mater Struct 1994;17(3):243–52.
[12] Wagner L. Mechanical surface treatments on titanium. aluminum and magnesium alloy. Mater Sci Eng 1999;A263:210–6.
[13] Benedetti M, Bortolamedi T, Fontanari V, Frendo F. Bending fatigue behavior of differently shot peened Al 6082 T5 alloy. Int J Fatigue 2004;26:889–97.
[14] Turnbull A, de los Rios ER, Tait RB, Laurant C, Boabaid JS. Boabaid JS. Improving the fatigue resistance of wasp alloy by shot peening. Fatigue Fract Eng Mater Struct 1998;21:1513–24.
[15] Luong H, Hill MR. The effects of laser peening and shot peening on high cycle fatigue in 7050–T7451 aluminum alloy. Mater Sci Eng A 2010;527:699–707.
[16] Wu BX, Tao S, Lei ST. Numerical modeling of laser shock peening with femtosecond laser pulses and comparisons to experiments. Appl Surf Sci 2010;256:4376–82.
[17] Gao YK. Improvement of fatigue property in 7050–T7451 aluminum alloy by laser peening and shot peening. Mater Sci Eng A 2011;528:3823–8.
[18] Cherif A, Pyoun Y, Scholtes B. Effects of ultrasonic nanocrystal surface modification (UNSM) on residual stress state and fatigue strength of AISI 304. J Mater Eng Perform 2010;19:282–6.
[19] Ramos R, Ferreira N, Ferreira JAM, Capela CAC. Batista AC. Improvement in fatigue life of Al 7475–T7351 alloy specimens by applying ultrasonic and microshot peening. Int J Fatigue 2016;92:87–95.
[20] Luo W, Noble B, Waterhouse RB. The effect of shot peening intensity on the fatigue and fretting behaviour of an aluminium alloy. Niku-Lari A, editor. Advances in Surface Treatments, vol. 2. Oxford: Pregamon Press; 1988. p. 145–53.
[21] Benedetti M, Fontanari V, Bandini M, Savio E. High- and very high-cycle plain fatigue resistance of shot peened high-strength aluminum alloys: The role of surface morphology. Int J Fatigue 2015;70:451–62.
[22] DIN EN ISO 4288, Profile method: Rules and procedures for the assessment of surface texture, 1996.
[23] Li JK, Mei Y, Wang D, Wang R. An analysis of stress concentration caused by shot peening and its application in predicting fatigue strength. Fatigue Fract Eng Mater Struct 1992;152:1271–9.
[24] Robertson GT. The Effect of shot size on the residual stresses resulting from shot peening. Shot Peener 1997;11(3):46–8.
[25] Murakami Y. Metal fatigue: effects os small defects and nommetallic inclusions. Elsevier Science; 2002.
[26] Dong P, Liu Z, Zhai X, Yan Z, Wang W, Liaw PK. Incredible improvement in fatigue resistance of friction stir welded 7075–T651 aluminum alloy via surface mechanical rolling treatment. Int J Fatigue 2019;124:15–25.
[27] He C, Yang K, Liu Y, Wang Q, Cai M. Improvement of very high cycle fatigue properties in an AA7075 friction stir welded joint by ultrasonic peening treatment. Fatigue Fract Engng Mater Struct 2017;40:460–8.